Cancer Stem Cells and Aneuploid Populations within Developing Tumors Are the Major Determinants of Tumor Dormancy

Anjali P. Kusumbe and Sharmila A. Bapat

National Centre for Cell Science, NCCS Complex, Pune University Campus, Ganeshkhind, Pune, India

Abstract

Tumor formation involves substantial cell division and genetic instability, but the relationship between quiescent cancer stem cells (CSC) and dividing progenitors in these events is poorly understood. Likewise, the implication of aneuploid cells in solid tumors is uncertain. CSCs are postulated to contribute to tumor dormancy and present a formidable obstacle in limiting treatment outcomes for a majority of cancers, whereas the genetic heterogeneity conjured by aneuploid cells may influence tumor drug resistance. However, direct confirmation of these events remains forthcoming. In the present study, we addressed the identification of tumor dormancy in terms of isolation of therapy-refractory residual tumor cells from tumors that persist in a state of quiescence as label-retaining cells. The choices of label were PKH67/PKH26 dyes that irreversibly bind to the lipid bilayer on cell membranes and get equally partitioned among daughter cells subsequent to each cell division. Consequent characterization revealed that label-retaining cells encompass two different populations capable of remaining in a state of quiescence, i.e., stem-like cells and aneuploid cells. The former express a reversibility of quiescence through retention of functionality and also exhibit therapeutic refractoriness; the latter seem to be either quiescent or proliferation-arrested at steady-state. Subsequent to exposure to selective pressure of chemotherapy, a fraction of these cells may acquire the potential to proliferate in a drug-refractory manner and acquire stem-like characteristics. Collectively, the findings of the present study reveal that tumor-derived CSCs and aneuploid populations contribute to drug resistance and tumor dormancy in cancer progression. [Cancer Res 2009;69(24):9245–53]

Introduction

Tumor dormancy represents a subclinical equilibrium achieved between host immunity and quiescent residual tumor cells (1), that can extend for up to decades after treatment followed by disease relapse (2, 3). Also interpreted as being the minimal residual disease, this state remains a major hurdle in achieving complete remission (4, 5). The exact identity and functional characterization of cells that contribute to tumor dormancy, i.e., the cellular components of minimal residual disease lesions remain poorly understood. In recent years, the association of tumor dormancy with cancer stem cells (CSC) has been extensively speculated following their identification in diverse cancers including breast, brain, ovary, prostate, etc. (6–9), based on their analogy with adult stem cells in terms of a high capacity for self-renewal and multi-lineage differentiation (10). A more primeval trait of stem cells in adult organs is quiescence, which is critical in tissue proliferation kinetics and maintaining tissue homeostasis (11). In an analogous manner, CSCs are speculated to remain quiescent; tumor dormancy is conjectured to correlate with this quiescent CSC fraction that is likely to persist posttherapy to drive disease relapse. Aneuploidy—described as a hallmark of cancer—is associated with proliferation defects and may impart selective, adaptive advantages under a specific permissive context to tumor cells (12, 13). This forms a strong case for aneuploid cells contributing to tumor dormancy. Unfortunately, a definitive identification of CSC and/or aneuploidy-related quiescence has remained elusive due to a paucity of experimental data.

Long-term label retention is widely used for the identification of stem cells (14–16). A standard label-retaining cell (LRC) assay exploits the slow-cycling nature of stem cells (the reason they retain their labels), whereas rapidly dividing, transit-amplifying (TA) progenitors generated through stem cell self-renewal (17), dilute their labels. LRCs thus represent experimentally marked slow-cycling stem cells. Although bromodeoxyuridine labeling of DNA is frequently used in LRC assays, recent studies show its cytotoxic nature (18). The use of membrane-labeling dyes such as PKH67/PKH26 that have a good correlation with bromodeoxyuridine incorporation and slow-cycling cells is suggested (19–21). These vital dyes consist of a fluorophore attached to an aliphatic carbon backbone that irreversibly binds to the lipid bilayer on cell membranes. Subsequent to each cell division, the label gets equally partitioned among daughter cells, resulting in the reduction of fluorescence intensity (22, 23). PKH labeling enables the monitoring of live cells and is useful when subsequent functional analysis of labeled cells is required (24). In the present study, we explored the application of PKH label retention/quenching as an effective readout for the identification of quiescent cells in tumors. Such an assessment revealed CSCs and aneuploidy as two contrasting nonproliferative states in tumors that can be coaxed into regeneration, thereby providing a novel understanding of the cellular determinants of tumor dormancy.

Materials and Methods

Cell lines, cell culture, and PKH labeling of cells. A4 cells used in the study were established earlier in our lab from malignant ascites of a patient diagnosed with grade 4 serous ovarian adenocarcinoma (10). Paclitaxel-resistant A4 cells (A4CR) were developed from parental A4 cells using standard procedures (25). Human tumor cell lines NT2, PA1, HL60, C6, U87, and T47D were obtained from the National Centre for Cell Science Repository and maintained as recommended. PKH labeling was performed as described earlier (24).

Note: Supplementary data for this article are available at Cancer Research Online (http://cancerres.aacrjournals.org/).

Requests for reprints: Sharmila A. Bapat, National Centre for Cell Science, NCCS Complex, Pune University Campus, Ganeshkhind, Pune 411 007, India. Phone: 91-020-25708074; Fax: 91-020-25692259; E-mail: sabapat@nccs.res.in.

doi:10.1158/0008-5472.CAN-09-2802

Animal housing, generation of tumors, and paclitaxel treatment. Nonobese diabetic (NOD)/severe combined immunodeficiency (SCID) mice were bred and maintained at the Experimental Animal Facility, National Centre for Cell Science; all procedures were done in accordance with institutional ethical animal committee clearances, laws, and policies. Animals were kept under sterile airflow conditions during the experiment. For subcutaneous tumor formation, either 4×10^6 unlabeled A4 cells (control group), or 4×10^6 PKH26 or PKH67-labeled A4 cells were injected s.c. into the thigh of 5- to 6-wk-old female NOD/SCID mice. Drug treatment of mice was with 25 mg/kg of paclitaxel, whereas vehicle control mice were exposed to DMSO (26). Further details of animal experiments are provided in the Supplementary Methods.

Tumor digestion for flow cytometry and analysis. Tumors were finely minced and subjected to collagenase digestion (collagenase IA and collagenase XI—both 5 mg/mL in RPMI medium) to obtain single-cell suspensions. CD44/c-kit staining and Ki67 staining were performed using standard protocols. PKH-based sorting was performed on FACSAria (Becton Dickinson) for semiquantitative PCR, quantitative PCR, clonogenicity, and tumorigenicity analyses. PKH intensity plots of labeled tumors yielded a continuous gradient of cells with high intensity similar to preinjected cells to cells devoid of label. PKH^{hi}, PKH^{lo}, and PKH^{neg} fractions were identified, gated, and sorted from this continuous gradient for subsequent analyses. Data analysis was with FACSDiva software.

Demarcation of euploid and aneuploid populations and distribution analysis of their cell cycle phases. Propidium iodide (PI)–based DNA content analysis does not resolve G_0 and G_1 cell cycle phases, which is achieved through Hoechst (DNA content)-Pyronin Y (RNA content) staining. Briefly, cells were stained using Hoechst 33342 (5 μg/mL for 45 min, at 37°C in staining buffer); 1 μg/mL of Pyronin Y was added and cells were incubated for an additional 45 min prior to washing and flow cytometry. Although Hoechst-Pyronin Y staining was applied for the identification of quiescent diploid stem cells from normal organs; it was not applied to tumor-derived cells that had heterogeneous DNA content. Our analysis of tumors indicated that whereas this staining enabled the demarcation of quiescent (G_0), euploid (P1), and quiescent (G_0) aneuploid (P2) fractions, euploid S – G_2/M and aneuploid G_1 phases (P4) merge on the histogram. Another drawback is that S – G_2/M phases are not resolved within the P5 fraction. PI staining however permits a lucid demarcation of S – G_2/M phases of euploid and aneuploid fractions. Thus, towards complete cell cycle profiling, both methods were performed, analyzed independently, and further overlapped to identify the frequencies of individual phases in euploid as well as aneuploid populations.

Semiquantitative and quantitative reverse transcription-PCR. Semiquantitative and quantitative reverse transcription-PCR was performed under standard conditions as described earlier (24).

Statistical analysis. Unless mentioned otherwise, all experiments were carried out in triplicate; data are expressed as mean ± SEM of at least three independent experiments. The significance of difference in the mean values was determined using two-tailed Student's t test. $P < 0.05$ was considered significant.

Results

Differential label retaining capacities suggestive of proliferation heterogeneity are expressed by cells within primary tumors and metastases. To visualize LRCs by flow cytometry, ovarian cancer cells (A4) were labeled with the membrane dye PKH67 and injected s.c. into NOD/SCID mice for tumor formation (Fig. 1*A, horizontal column*; Materials and Methods). Analyses of 3-week-old tumors (n = 11) for distribution of PKH intensity revealed a continuous gradient of cells with fluorochrome PKH67 retention ranging from high (PKH^{hi}, equivalent to preinjected cells), low (PKH^{lo} cells), to total label quenching (PKH^{neg}; Fig. 1*A, vertical column*). Such profiles could be consistently identified in all tumors (n = 25) ranging from short-term (2 weeks) to fairly long-term (6 weeks). However, the cell distribution frequencies of each fraction varied between short-term and long-term tumors, with the size of the PKH^{hi} fraction diminishing with tumor progression (Supplementary Fig. S1*A*); this could partly be an effect of increasing tumor mass with time. Ovarian cancer progression is characterized by the formation of malignant ascites and the development of secondary peritoneal tumors; the A4 cells model this pattern in immunocompromised mice (10). Our next attempt was to decipher label retention during tumor progression. PKH67-labeled A4 cells were injected i.p. in NOD/SCID mice; 40 days postinjection, multilayered spheroids, single cells within the ascites and secondary tumors, were collected, digested, and analyzed by flow cytometry and/or immunofluorescence. All metastases-derived cells showed the three cell fractions differentiated on the basis of their label retention (Supplementary Fig. S1*B*). To further elucidate whether the PKH-based gradient identified in A4-derived tumors is cell type–specific or represents a general scheme during tumor formation, we analyzed 3-week-old tumors (n = 3) generated in NOD/SCID mouse models from PKH67-labeled C6 cells (a rat glioma–derived cell line). Consequently, the three fluorochrome-based cell subsets differentiated in A4 cells were also identified in C6-derived tumors (Supplementary Fig. S1*C*). Because label quenching is a direct function of fluorochrome dilution following each consecutive cell division, the profiles generated are strongly suggestive of the subsistence of proliferative heterogeneity within primary tumors and their metastases consisting of three distinct populations: (*a*) label-retaining PKH^{hi} cells suggested to be slow-cycling/quiescent, (*b*) PKH^{lo} cells that undergo partial label dilution indicative of limited divisions, and (*c*) PKH^{neg} cells that undergo total dye quenching suggestive of consecutive, rapid divisions.

Label-retaining PKH^{hi} cells exhibited the highest self-renewal potential and stem cell marker expression. To correlate between slow-cycling, proliferation, and self-renewal capabilities, the three freshly sorted PKH tumor cell fractions were subjected to colony formation assays *in vitro* and tumorigenicity *in vivo*. The clonogenic potential of PKH^{hi} cells was significantly higher than that of PKH^{lo} cells, whereas the PKH^{neg} subset lacked colony formation potential (Fig. 1*B, top*). *In vivo*, the high tumorigenic nature of the PKH^{hi} subset was clearly shown wherein only 5,000 cells were capable of initiating and developing tumors in all animals injected (Fig. 1*B, bottom*). The minimal threshold of tumor initiation for the PKH^{lo} subset was ~10,000 cells; whereas PKH^{neg} cells failed to display tumorigenic potential. These analyses indicated that the tumor-initiating capacity of the A4 population lies primarily within the PKH^{hi}, and to a lesser extent, in the PKH^{lo} subset. The three tumor cell subsets were also screened for expression of stem cell markers *Oct4, Nestin, Nanog,* and *Bmi. Oct4* and *Nestin* expressions were exclusively associated with the PKH^{hi} subset, whereas *Nanog* and *Bmi* were expressed in PKH^{hi} and PKH^{lo} subsets with expressions being higher in the former (Fig. 1*C, top*). The PKH^{neg} subset lacked expression of all four markers. On studying the association of a recently described cell surface phenotype of ovarian CSCs (CD44+/c-kit+; ref. 27) with the three tumor cell subsets, these expressions were totally absent in the PKH^{neg} subset, whereas 68% of PKH^{lo} and the entire PKH^{hi} subset were enriched for double-positive expression (Fig. 1*C, bottom*). We also probed the expression of the proliferation marker Ki67 (expressed in late G_1, S, and G_2/M phases of cell cycle) in these fractions. Approximately half (57%) of the PKH^{lo} subset and 7% of PKH^{hi} and 7.1% of PKH^{neg} cells expressed Ki67 (Fig. 1*D*). In totality, our results suggest that the PKH^{hi} subset represents label-retaining, slow-cycling stem-like cells; the PKH^{lo} subset as a progenitor population (most

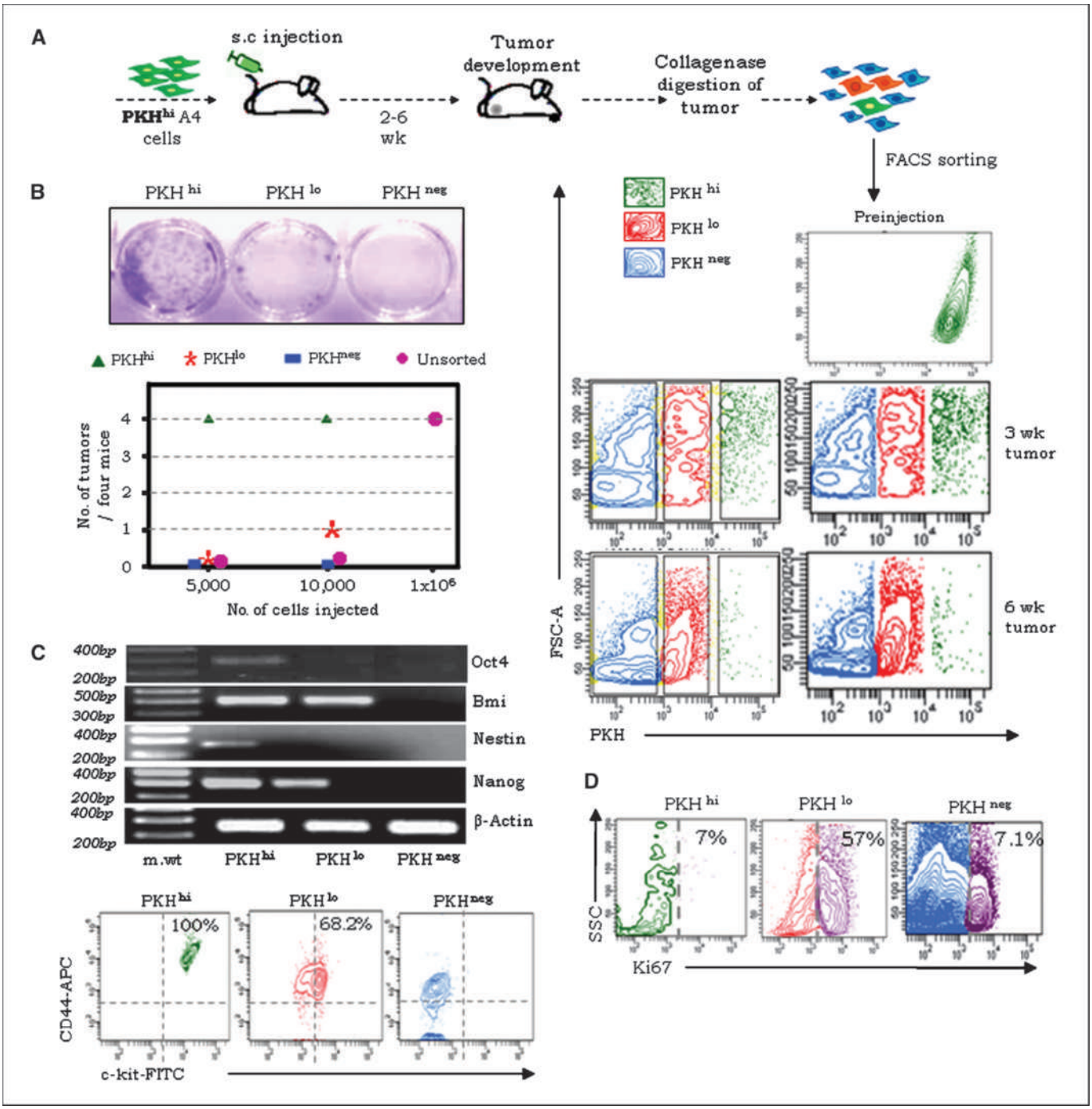

Figure 1. Identification of LR-CSCs within the tumors. *A,* experimental design for PKH label based on *in vivo* detection of quiescent cells within tumors. Representative PKH intensity profiles of preinjected cells, 3- and 6-wk A4 tumors. *B,* clonogenic potential of tumor-derived PKH^{hi}, PKH^{lo}, and PKH^{neg} cells (*top*). Tumorigenicity of these fractions and unsorted A4 cells transplanted s.c. into NOD/SCID mice (*bottom*). *C,* semiquantitative PCR analyses (*top*) of stem cell markers in the three PKH cell populations; β-actin mRNA expression used as internal control. *D,* representative contour plots of flow cytometric analysis for expression of ovarian CSC markers c-kit/CD44 (*bottom*) and proliferation marker Ki67 in the PKH subsets.

likely TA progenitors); and the PKH^{neg} subset as the differentiated fraction within tumors (the latter may additionally harbor some host-derived cells that would not express the label).

The PKH^{lo} subset comprised of proliferation-arrested aneuploid cells and euploid progenitor cells. PI-based cell cycle analyses of 3-week-old tumor-derived cells further confirmed the proliferation kinetics of the three subsets and lent support to the above classification identified through functional and phenotypic expression analyses (Fig. 2*A*). Although the PKH^{lo} fraction seems to represent the immediate progeny of PKH^{hi} CSCs, a striking feature revealed from the PI profiles was that a major fraction of these cells expressed enhanced ploidy levels (DNA content 4N or more as compared with baseline A4 euploid DNA levels). Such aneuploid cells were also present in the PKH^{hi} population albeit to a lesser extent, but did not appear in the PKH^{neg} fraction. The absence of such cells prior to injection (Supplementary Fig. S2*A*) suggested the

association of *in situ* tumor development with genetic instability and rearrangements that could lead to the emergence of aneuploidy. These processes are identified as hallmarks of tumorigenesis (12); however, their existence was further affirmed through DNA content analysis of primary ovarian cancer samples (eight tumors and one malignant ascites) that harbored 1.87% to 6.74% (mean = 4.16 ± 1.54%) aneuploid cells (Supplementary Fig. S2*B* and *C*). To further correlate between ploidy levels and cell cycle phases, we supplemented the PI-generated profiles with those generated through Hoechst-Pyronin Y staining. The various cell cycle phases of euploid and aneuploid populations were gated based on their DNA content as indicated (Fig. 2*B*), and included—P1 (euploid G_0), P2 (aneuploid G_0), P3 (euploid G_1), P4 (aneuploid G_1 + euploid G_2/M), and P5 (aneuploid S + G_2/M). Combinatorial PI and Hoechst-Pyronin Y analysis clearly revealed the lack of an S phase within the aneuploid population along with the persistence of large fractions of cells in G_1 and G_2/M phases, thereby suggesting the subsistence of proliferation arrest within the aneuploid compartment of tumors (Fig. 2*C*). Most significantly, a distinct fraction of quiescent (G_0) aneuploid cells was consistently detected in all the tumors analyzed.

To confirm the correlation of aneuploidy with cell cycle arrest, we examined the transcript levels of cell cycle inhibitors (*p14, p16, p21, p27,* and *p57*) and *MDM2* (negative regulator of *p53*) within

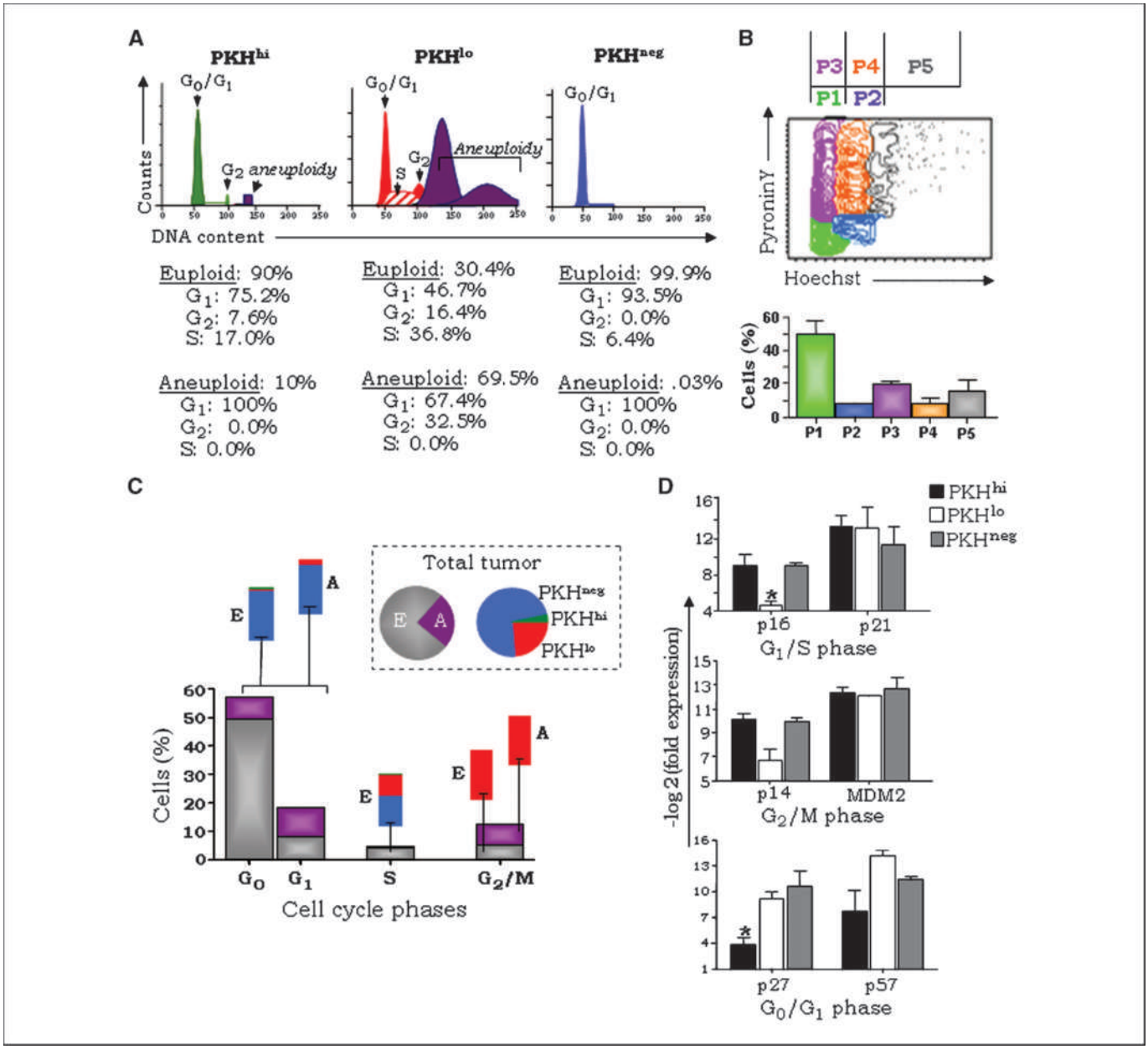

Figure 2. Aneuploidy constitutes a nonproliferative subset within tumors. *A,* PI-based DNA content analysis of tumor-derived PKH subsets. The percentage distribution of different cell cycle phases within euploid and aneuploid fractions (*bottom*). *B,* representative contour plot for Hoechst-Pyronin Y staining–based cell cycle analyses; P1 to P5 demarcated distinct gates as indicated above the plot: P1, euploid G_0 fraction; P2, aneuploid G_0; P3, euploid G_1; P4, euploid S + G_2/M and aneuploid G_1; P5, aneuploid S – G_2/M phases; *columns,* percentages of each fraction. *C, columns,* mean cell cycle phases within euploid and aneuploid fractions identified through combinatorial analyses of PI and Hoechst-Pyronin Y staining; *bars,* contributions of the three PKH subsets to these phases. *D,* real-time PCR to detect expression levels (ΔCt expression values) of cell cycle checkpoints in the three PKH subsets; β-actin used as an internal control (*, $P < 0.05$).

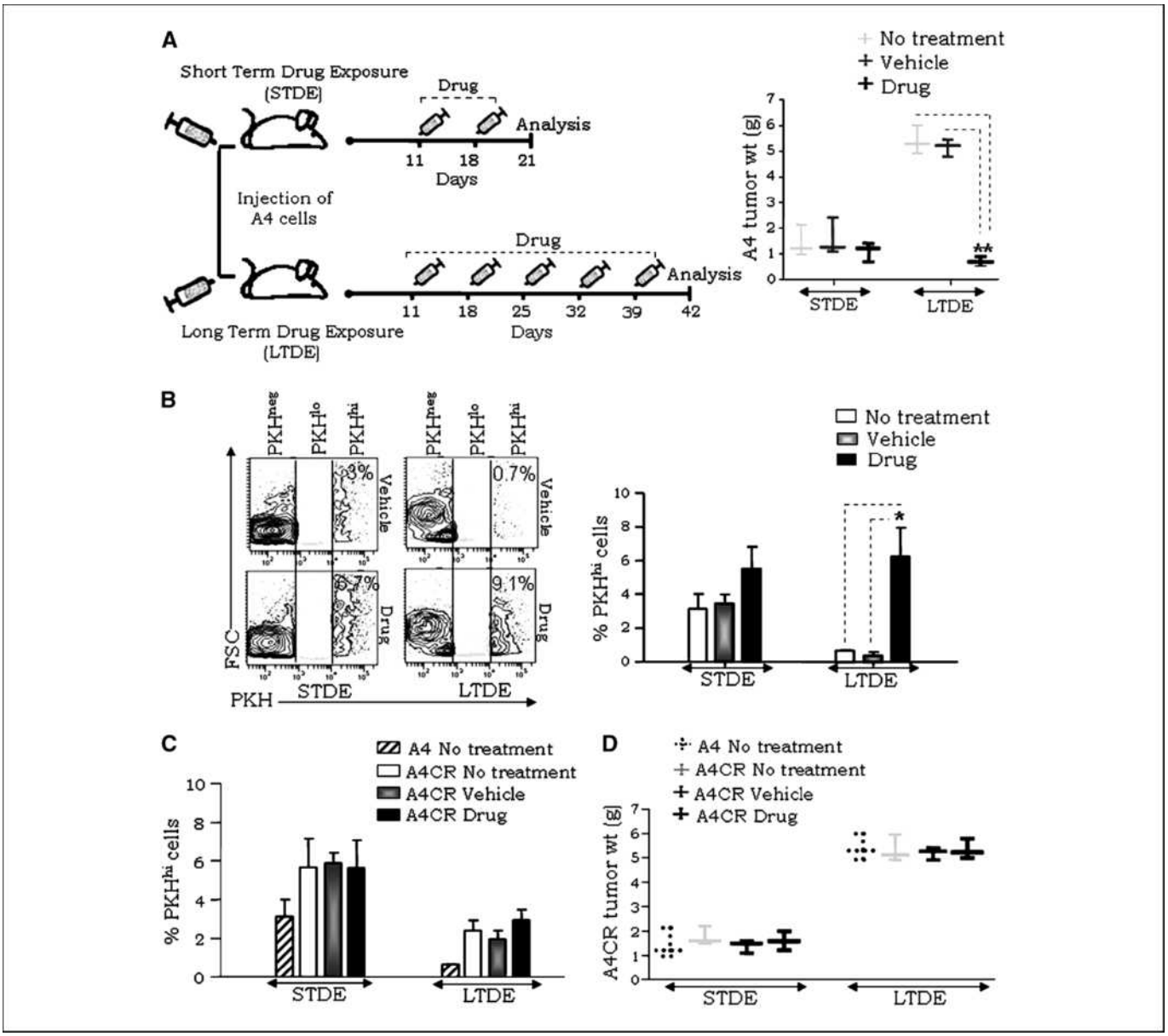

Figure 3. Chemotherapy leads to the enrichment of LR-CSCs within tumors. *A, left,* experimental design adapted for drug treatment (STDE, 3 wk; LTDE, 6 wk); *right,* line plots represent A4 tumor weights in untreated, vehicle (DMSO) controls, or paclitaxel-treated NOD/SCID mice (**, $P < 0.01$). *B, left,* representative dot plots of PKH^{hi} cell frequency within A4 tumors under drug treatments/controls; *right,* bar graphs representing *C* (*, $P < 0.05$). *C, columns,* A4CR tumor weights in untreated, vehicle control, or paclitaxel-treated NOD/SCID mice; parental A4 tumor weights were included for comparison. *D,* bar graphs indicating the PKH^{hi} cell frequency within A4CR tumors harvested after drug treatment as compared with untreated/vehicle controls/parental A4 tumors.

the three PKH67-demarcated subsets. *p16*—G_1-S and *p14*—G_2/M arrest, respectively (28, 29), were found to be elevated in the PKH^{lo} subset; significant upregulation of *p27* in the PKH^{hi} CSCs and not by the PKH^{neg} cells provided the subtle distinction between cell cycle exit of quiescent PKH^{hi} versus that of differentiated PKH^{neg} subsets (Fig. 2*D*). Final validation of the proliferation inability of the tumor-derived aneuploid cells within the PKH^{lo} subset came from their lack of proliferation (Supplementary Fig. S2*D*) and low clonogenic index when brought into culture (Supplementary Fig. S2*E*). The former was derived from the fact that upon sorting the PKH^{lo} subset from A4 tumors ($n = 3$), and maintenance in culture, a complete depletion of the aneuploid fraction was evident within a few passages. Collectively, these results identify a proliferation arrest in the aneuploid cell fraction in tumors. This data is in concordance with recent studies that identify a negative role for aneuploidy in cellular proliferation (13).

Chemotherapy leads to the enrichment of quiescent CSCs that retain their functionality upon removal of selective pressure. The identification of CSCs as LRCs that undergo reversible quiescence provided the first indication of their involvement in tumor dormancy. Furthermore, the survival and persistence of their functionality during therapeutic regimes would provide a defining validation. We thereby assessed the outcome of chemotherapy on the quiescent, label-retaining PKH^{hi} subset in drug-treated tumors. NOD/SCID mice injected (s.c) with PKH-labeled A4 cells were subsequently administered paclitaxel under two treatment regimes,

i.e., short-term and long-term exposures (STDE and LTDE, respectively; Fig. 3*A, left*), whereas vehicle control groups were treated with DMSO (Materials and Methods). Drug effects were not evident in STDE, because the tumor size remained comparable to those in the controls (Fig. 3*A, right*). However, under LTDE, tumors stopped growing, and marginally reduced in size as compared with those at 3 weeks indicating long-term cytotoxic effects. Thus, higher treatment efficacies are suggested in the LTDE over STDE group.

If the quiescence of CSCs operates like a safeguard mechanism against therapy, drug exposure could lead to the accumulation of LRCs. Our results conformed to this reasoning as paclitaxel administration augmented PKH^{hi} cells within STDE and LTDE tumors (Fig. 3*B, left* and *right*). It is likely that the elevated numbers of PKH^{hi} CSCs in STDE tumors represent an initiation of drug-induced enrichment that is further enhanced on continuing treatment in LTDE tumors. We had earlier determined that the PKH^{hi} label is retained for up to three to four divisions *in vitro*, after which it undergoes quenching to enter the PKH^{lo} fraction (Supplementary Fig. S3*A*). An active enrichment of CSCs involving self-renewal through a few minimal divisions is thus possible without inducing sufficient PKH label quenching that could drive these cells into the PKH^{lo} subset. Cell cycle analyses (PI staining) of A4-derived STDE and LTDE tumors showed enhanced G_0-G_1 in the euploid fraction (Fig. 4*A, left*); consequent Hoechst-Pyronin Y analyses elucidated that a significant amount of increase localized to the G_0 rather than in the G_1 phase (Fig. 4*A, right*). This analysis further supported the fact that tumor treatment leads to the accumulation of euploid cells in a quiescent state. Subsequent clonogenicity analysis of sorted PKH^{hi} cells from STDE and LTDE tumors showed posttherapy reversion of drug-induced quiescence in tumor-derived PKH^{hi} cells that retained their functionality (Supplementary Fig. S4*A*). This, along with a significant increase in the PKH^{hi} subset in drug-exposed tumors supports our perception that the augmentation of quiescent cells within drug-treated tumors involves active enrichment of functional CSCs and is not a consequence of drug-mediated accumulation of label-retaining

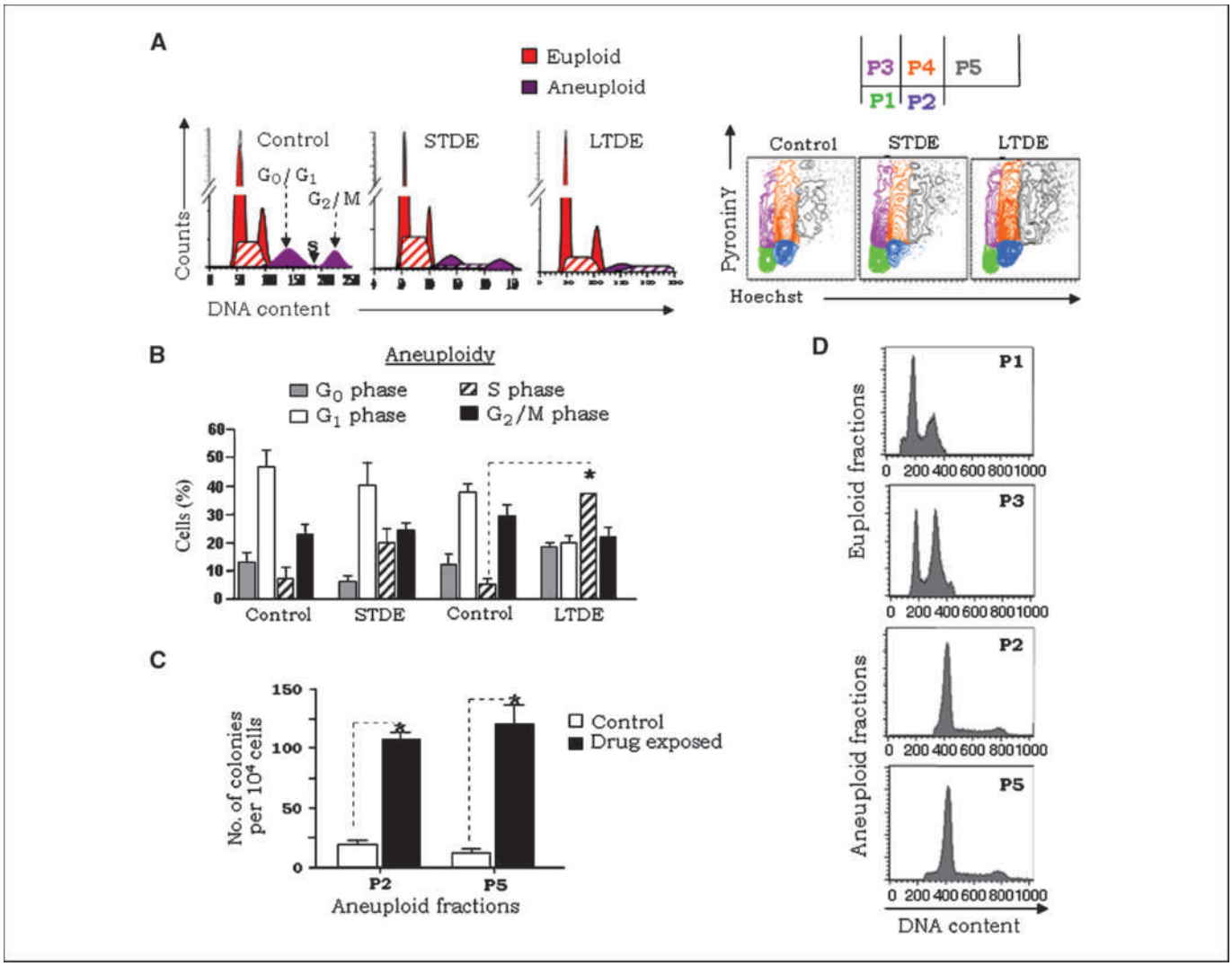

Figure 4. Chemotherapy triggered proliferation within the aneuploid compartment. *A, left,* representative histograms of PI-based DNA content analysis of treated and control tumors; *right,* representative Hoechst-Pyronin Y staining dot plot of A4 untreated or treated tumors. *B, columns,* cell cycle phase frequencies within aneuploid fractions identified through combinatorial PI and Hoechst-Pyronin Y staining. *C, columns,* clonogenic potential of aneuploid fractions P2 and P5 from untreated and paclitaxel-treated tumors (*, $P < 0.05$). *D,* representative DNA content analysis of the sorted and cultured P1 (euploid G_0), P3 (euploid G_1), P2 (aneuploid G_0), and P5 (aneuploid S + G_2/M) fractions from paclitaxel-treated tumors.

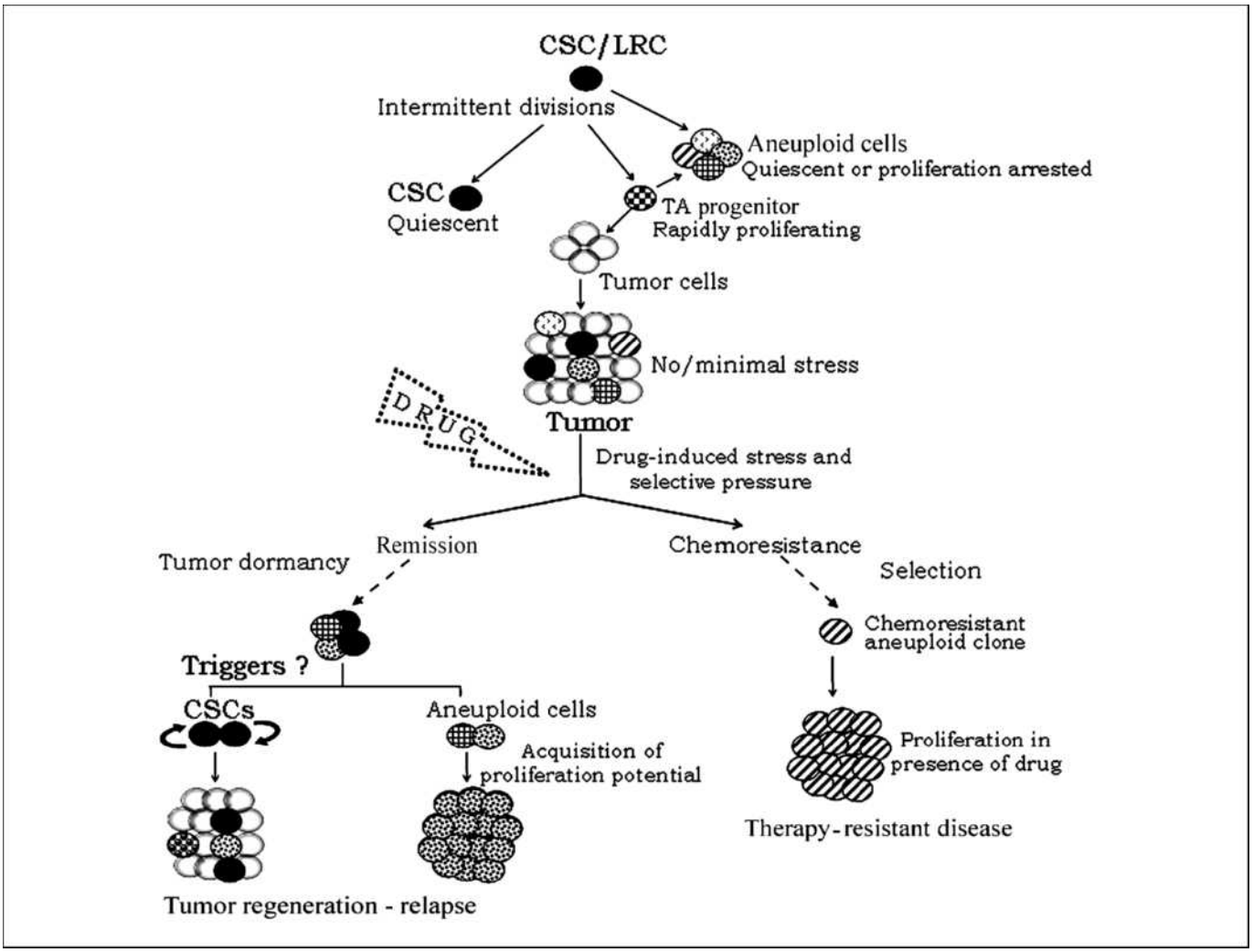

Figure 5. Schematic illustrating the contribution of CSCs and aneuploid populations to tumor dormancy.

senescent or apoptotic cells. Recently, the role of transcription factors Snail and Slug in enriching CSCs under radioresistance and chemoresistance was reported from our lab (28); chemoresistant A4 cells (termed A4CR, resistant to 400 ng of paclitaxel; LD_{50} for parental A4 cells was 60 ng) were shown to harbor higher frequencies of CSCs as compared with parental cells at steady-state. In the current study, we identified that these drug-resistant cells also exhibited a higher label-retention capacity *in vitro* (Supplementary Fig. S4*B*) and *in vivo* (Fig. 3*C*); however, A4CR-derived tumors under a paclitaxel regime do not undergo further LRC enrichment and were not growth-restricted (size) as compared with control tumors (Fig. 3*D*). This reflects a drug-tolerant stage under which chemoresistant cells achieve steady-state tumor growth.

Chemotherapy coaxes aneuploid cells out of their quiescent/proliferation-arrested states due to selective pressure. Our observations in developing tumors were that aneuploid cells tend to accumulate in the PKH^{lo} subset either due to quiescence or proliferation arrest. This identifies them as potential cellular candidates that could contribute to tumor dormancy, survival, and regeneration. In assessing this postulate, we studied the outcome of chemotherapy on these cells in drug-treated tumors as above (STDE and LTDE). Although the number of aneuploid cells seemed to decrease under both paclitaxel treatment regimes, cell cycle analyses revealed the emergence of a distinct S phase fraction within the aneuploid subset (Fig. 4*A, left*). Furthermore, Hoechst-Pyronin Y resolution identified a higher fraction of cells in G_0 and S – G_2/M phases (Fig. 4*A, right*). Combining these analyses, we concluded that a redistribution of aneuploid cells occurs upon exposure to paclitaxel, leading to an increase of cells in G_0 and S phases, and decreased G_1 and G_2/M phases (Fig. 4*B*). This is a major difference between control tumor-generated aneuploid cells that were likely to be arrested in G_0-G_1 or G_2/M phases (Fig. 2*A*), and those in paclitaxel-exposed tumors that seem to re-enter the cell cycle albeit at very low frequencies, whereas a major portion of these cells might be affected by the drug. The reduction of post-treatment aneuploidy in the PKH^{lo} fraction may thus be attributed to a reinstating of proliferation-induced label quenching within this population that was previously trapped within the PKH^{lo} subset (Supplementary Fig. S4*C*). A functional evaluation of this potential in aneuploid fractions P2 (G_0) and P5 (S + G_2/M) sorted from paclitaxel-treated tumors based on Hoechst-Pyronin Y staining, identified increased clonogenic potential as compared with untreated tumors (Fig. 4*C*). Further profiling the DNA content of

colonies formed *in vitro* by these fractions confirmed the cycling of aneuploid clones (Fig. 4*D*).

Discussion

Quiescence prevents stem cell exhaustion in normal tissues (30). In contrast to other nonproliferative states (terminal differentiation/senescence), only quiescent stem cells retain the ability to resume proliferation (31). Thereby, quiescence and its reversibility become defining parameters of stem cells. These characteristics have been speculated on extensively in the context of CSCs, especially with regard to drug evasion, but has never actually been experimentally shown. Thereby, the objectives of the present study were to (*a*) develop a convenient readout for the identification of quiescent cell fractions in an experimental model of tumor development, (*b*) functionally characterize these quiescent populations that distinguish them from other nonproliferative states, and (*c*) analyze their effects under drug treatment.

Through a convenient readout of label retention, we thus showed that stem cell activity is enriched in the quiescent fraction of a tumor that shows the capability to revert to a state of self-renewal and regeneration. Classically, CSC isolation from tumors exploits the detection of cell surface markers associated with normal stem cells. However, disparities in such approaches have been noted (32, 33), especially because quiescence has not been shown in these cells. Moreover, although surface markers provide obvious advantages, a single phenotype cannot account for the heterogeneity within CSC populations (34–36). Our results further indicate that a specific surface expression may not be exclusively associated with CSCs, but also encompasses progenitor and aneuploid populations. In understanding the events that lead to tumor dormancy, it is imperative to subject putative CSCs to a functional assessment such as quiescence and/or drug resistance capabilities rather than surface phenotypes. Besides harboring CSCs, most solid tumors contain aneuploid populations that represent genetically diverse cell pools with reduced cell proliferation and cellular fitness (13). In a small subset of such cells, however, cellular imbalances associated with increased mutation rate, gene amplification, and/or genomic instability have linked aneuploidy with tumor dormancy (37, 38). On this background, our observations clearly illustrate (*a*) the stem-like potential of tumor-derived LRCs to survive, persist, and retain functionality through drug regimes; thereby contributing to tumor dormancy; and (*b*) acquisition of proliferation potential by quiescent/cell cycle–arrested aneuploid cells through a re-entry into the cell cycle to contribute to disease progression. Chemotherapy-imposed selective pressures could trigger this response which exploits intrinsic survival capabilities to finally result in a phenotypic switch. Additional acquisition of stem-like characteristics by such a clone ensures its long-term survival and potential contribution to tumor dormancy (Fig. 5).

Prompted by the detection of LR-CSCs within tumors, we also attempted to detect LRCs in cancer cell lines *in vitro*. Towards this end, the A4 cells were membrane-labeled with PKH, cultured and harvested at regular intervals (48 hours) for analyses of label intensities by flow cytometry. By 78 hours, a large bulk of cells underwent quenching of label intensity (Supplementary Fig. S3*A*). Two groups could be demarcated within the bulk cells based on differential label intensities that correspond with different proliferation rates; we termed these two populations as lagging (slow) and leading (fast) groups (Supplementary Fig. S4*A* and *B*). However, these subtle proliferative differences *in vitro* did not seem to have the same significance as quiescent cells *in situ*, as further monitoring revealed that the entire population of cells in culture underwent a complete quenching of label by 264 hours (Supplementary Fig. S4*A*). In addition to A4 cells, we also analyzed the proliferation profiles of NT2, C6, U87, HL60, PA1, and T47D cell lines. All these cells, under defined culture conditions, showed an analogous pattern of proliferation marked by the absence of LRCs/PKH^{hi} subset (Supplementary Fig. S3*C*). Thus, in contrast to their growth *in situ*, cultured cells seem to be devoid of LRCs, probably due to use of culture conditions optimized for cell proliferation. As a corollary, tumor-derived quiescent PKH^{hi} cells, when brought into culture, showed a high clonogenic capability. The intrinsic quiescence of cells *in vitro* is however not irreversibly lost, but can be recapitulated *in situ* where niche elements exert their instructive role. Thereby, the "stem-like" cells in tumors result from effects of intrinsic and extrinsic elements during tumor formation. A similar situation is observed in case of aneuploid cells that are associated with developing tumors and do not proliferate rapidly in culture. Our observations receive support from previous studies proposing that the reciprocal interaction between the tumor cells and microenvironment controls the switch between proliferation and quiescence (3, 39, 40).

Quiescent LR-CSCs undergo intermittent divisions leading to self-renewal and generation of rapidly proliferating TA progenitors (that reside within the PKH^{lo} subset and subsequently give rise to the bulk tumor—PKH^{neg} cells; Fig. 5). Genetic instability during such divisions may also generate aneuploid CSC progenitor clones (38). These aneuploid populations, akin to the CSCs, also constitute a dormant subset within tumors either through quiescence or a proliferation arrest. Therapy may eradicate TA cells because most drugs target proliferative cells; concurrently, the differentiated bulk tumor cells also perish, ultimately leading to tumor shrinkage. Thus, drug exposure leads to two possibilities—a dormant aneuploid clone refractile to drug effects might emerge to drive aggressive disease progression, or remission ensues, reflecting an initial high therapeutic efficacy. However dormant, therapy-refractive CSCs and aneuploid CSCs may persist within the host as minimal residual disease. The triggering of these cellular elements defining tumor dormancy from their state of quiescence is not understood as yet, but their capability to lead to disease relapse is recognizable from the results presented here.

Our findings also indicate that the cellular dormancy program in tumor-derived LR-CSCs and aneuploid cells might be dominant over oncogenic signaling, thereby ensuring their survival in a quiescent state. Tumor dormancy complements the selection of a chemoresistant clone that is likely to be aneuploid to provide the genetic variability for drug-resistant growth and acquisition of stem cell characteristics. Several mechanisms are possibly involved, e.g., expression of multidrug resistance proteins, increased resistance to drug-mediated apoptosis, tumor stroma–mediated acquisition of drug resistance, etc. (41–43). From a clinical perspective, our findings illustrating the contribution of CSCs and aneuploid populations to tumor dormancy has significant therapeutic implications, but presents a major challenge because the multidrug resistance exhibited by the CSCs and unstable karyotype confers intangible, adaptive advantages to aneuploid cells. Thus, it becomes increasingly important to further decipher the interactions and systemic signals that govern the maintenance of the dormant state and the switch between dormancy and proliferation in these cells, including exploiting the putative niche that nurtures the CSCs and their aneuploid progeny as drug targets.

Disclosure of Potential Conflicts of Interest

No potential conflicts of interest were disclosed.

Acknowledgments

Received 7/29/09; revised 9/25/09; accepted 10/16/09; published OnlineFirst 12/1/09.

Grant support: Department of Biotechnology, Ministry of Science and Technology, Government of India, New Delhi.

The costs of publication of this article were defrayed in part by the payment of page charges. This article must therefore be hereby marked *advertisement* in accordance with 18 U.S.C. Section 1734 solely to indicate this fact.

We thank Dr. G.C. Mishra, Director, National Centre for Cell Science (Pune, India) for encouragement and support; Nimisha Singh for technical assistance in Supporting Information S3; and N.K. Kurrey for providing A4CR cells. Assistance from the NCCS Animal, FACS, and Confocal Facilities is gratefully acknowledged. A.P. Kusumbe receives a fellowship from the Council of Scientific and Industrial Research, New Delhi.

References

1. Quesnel B. Tumor dormancy and immunoescape. APMIS 2008;116:685–94.
2. Holmgren L, O'Reilly MS, Folkman J. Dormancy of micrometastases: balanced proliferation and apoptosis in the presence of angiogenesis suppression. Nat Med 1995;1:149–53.
3. Aguirre-Ghiso JA. Models, mechanisms and clinical evidence for cancer dormancy. Nat Rev Cancer 2007;7:834–46.
4. Crowley NJ, Seigler HF. Relationship between disease-free interval and survival in patients with recurrent melanoma. Arch Surg 1992;127:1303–8.
5. Demicheli R, Abbattista A, Miceli R, Valagussa P, Bonadonna G. Time distribution of the recurrence risk for breast cancer patients undergoing mastectomy: further support about the concept of tumor dormancy. Breast Cancer Res Treat 1996;41:177–85.
6. Al Hajj M, Wicha MS, Benito-Hernandez A, Morrison SJ, Clarke MF. Prospective identification of tumorigenic breast cancer cells. Proc Natl Acad Sci U S A 2003;100:3983–8.
7. Singh SK, Hawkins C, Clarke ID, et al. Identification of human brain tumour initiating cells. Nature 2004;432:396–401.
8. Bapat SA, Mali AM, Koppikar CB, Kurrey NK. Stem and progenitor-like cells contribute to the aggressive behavior of human epithelial ovarian cancer. Cancer Res 2005;65:3025–9.
9. Collins AT, Berry PA, Hyde C, Stower MJ, Maitland NJ. Prospective identification of tumorigenic prostate cancer stem cells. Cancer Res 2005;65:10946–51.
10. Blanpain C, Lowry WE, Geoghegan A, Polak L, Fuchs E. Self-renewal, multipotency, and the existence of two cell populations within an epithelial stem cell niche. Cell 2004;118:635–48.
11. Yahata T, Muguruma Y, Yumino S, et al. Quiescent human hematopoietic stem cells in the bone marrow niches organize the hierarchical structure of hematopoiesis. Stem Cells 2008;26:3228–36.
12. Rajagopalan H, Lengauer C. Aneuploidy and cancer. Nature 2004;432:338–41.
13. Williams BR, Prabhu VR, Hunter KE, et al. Aneuploidy affects proliferation and spontaneous immortalization in mammalian cells. Science 2008;322:703–9.
14. Yue Z, Jiang TX, Widelitz RB, Chuong CM. Mapping stem cell activities in the feather follicle. Nature 2005;438:1026–9.
15. Levy V, Lindon C, Harfe BD, Morgan BA. Distinct stem cell populations regenerate the follicle and interfollicular epidermis. Dev Cell 2005;9:855–61.
16. Tumbar T, Guasch G, Greco V, et al. Defining the epithelial stem cell niche in skin. Science 2004;303:359–63.
17. Bapat SA. Evolution of cancer stem cells. Semin Cancer Biol 2007;17:204–13.
18. Ross HH, Levkoff LH, Marshall GP, et al. Bromodeoxyuridine induces senescence in neural stem and progenitor cells. Stem Cells 2008;26:3218–27.
19. Boyd FT. Identification of growth inhibited cells by retention of a lipophilic fluorescent dye. Cell Growth Differ 1993;4:777–84.
20. Lanzkron SM, Collector MI, Sharkis SJ. Hematopoietic stem cell tracking *in vivo*: a comparison of short-term and long-term repopulating cells. Blood 1999;93:1916–21.
21. Boutonnat J, Faussat AM, Marie JP, et al. Usefulness of PKH fluorescent labelling to study leukemic cell proliferation with various cytostatic drugs or acetyl tetrapeptide-AcSDKP. BMC Cancer 2005;5:120.
22. Horan PK, Melnicoff MJ, Jensen BD, Slezak SE. Fluorescent cell labeling for *in vivo* and *in vitro* cell tracking. Methods Cell Biol 1990;33:469–90.
23. Boutonnat J, Barbier M, Muirhead K, et al. Response of chemosensitive and chemoresistant leukemic cell lines to drug therapy: simultaneous assessment of proliferation, apoptosis, and necrosis. Cytometry 2000;42:50–60.
24. Kusumbe AP, Mali AM, Bapat SA. CD133-expressing stem cells associated with ovarian metastases establish an endothelial hierarchy and contribute to tumor vasculature. Stem Cells 2009;27:498–508.
25. Kurrey NK, Jalgaonkar SP, Joglekar AV, et al. Snail and Slug mediate radio- and chemo-resistance by antagonizing p53-mediated apoptosis and acquiring a stem-like phenotype in ovarian cancer cells. Stem Cells 2009;27:2059–68.
26. Colombo T, Parisi I, Zucchetti M, Sessa C, Goldhirsch A, D'Incalci M. Pharmacokinetic interactions of paclitaxel, docetaxel and their vehicles with doxorubicin. Ann Oncol 1999;10:391–5.
27. Zhang S, Balch C, Chan MW, et al. Identification and characterization of ovarian cancer-initiating cells from primary human tumors. Cancer Res 2008;68:4311–20.
28. Carnero A, Hudson JD, Price CM, Beach DH. p16INK4A and p19ARF act in overlapping pathways in cellular immortalization. Nat Cell Biol 2000;2:148–55.
29. Stott FJ, Bates S, James MC, et al. The alternative product from the human CDKN2A locus, p14ARF, participates in a regulatory feedback loop with p53 and MDM2. EMBO J 1998;17:5001–14.
30. Orford KW, Scadden DT. Deconstructing stem cell self-renewal: genetic insights into cell-cycle regulation. Nat Rev Genet 2008;9:115–28.
31. Sang L, Coller HA, Roberts JM. Control of the reversibility of cellular quiescence by the transcriptional repressor HES1. Science 2008;321:1095–100.
32. Shmelkov SV, Butler JM, Hooper AT, et al. CD133 expression is not restricted to stem cells, and both CD133+ and CD133– metastatic colon cancer cells initiate tumors. J Clin Invest 2008;118:2111–20.
33. Jordan CT. Cancer stem cells: controversial or just misunderstood? Cell Stem Cell 2009;4:203–5.
34. Beier D, Hau P, Proescholdt M, et al. CD133+ and CD133– glioblastoma-derived cancer stem cells show differential growth characteristics and molecular profiles. Cancer Res 2007;67:4010–5.
35. Wright MH, Calcagno AM, Salcido CD, Carlson MD, Ambudkar SV, Varticovski L. Brca1 breast tumors contain distinct CD44+/CD24– and CD133+ cells with cancer stem cell characteristics. Breast Cancer Res 2008;10:R10.
36. Visvader JE, Lindeman GJ. Cancer stem cells in solid tumours: accumulating evidence and unresolved questions. Nat Rev Cancer 2008;8:755–68.
37. Weaver BA, Cleveland DW. Aneuploidy: instigator and inhibitor of tumorigenesis. Cancer Res 2007;67:10103–5.
38. Sieber OM, Heinimann K, Tomlinson IP. Genomic instability-the engine of tumorigenesis? Nat Rev Cancer 2003;3:701–8.
39. Weaver VM, Petersen OW, Wang F, et al. Reversion of the malignant phenotype of human breast cells in three-dimensional culture and *in vivo* by integrin blocking antibodies. J Cell Biol 1997;137:231–45.
40. White DE, Kurpios NA, Zuo D, et al. Targeted disruption of β1-integrin in a transgenic mouse model of human breast cancer reveals an essential role in mammary tumor induction. Cancer Cell 2004;6:159–70.
41. Johnstone RW, Ruefli AA, Smyth MJ. Multiple physiological functions for multidrug transporter P-glycoprotein? Trends Biochem Sci 2000;25:1–6.
42. Kulawiec M, Owens KM, Singh KK. Cancer cell mitochondria confer apoptosis resistance and promote metastasis. Cancer Biol Ther 2009;8:1378–85.
43. Burger JA, Peled A. CXCR4 antagonists: targeting the microenvironment in leukemia and other cancers. Leukemia 2009;23:43–52.